Simulation of coherent energy transfer in an α-helical peptide by Fermi resonance

David L. Clarke and Michael A. Collins
Research School of Chemistry, Australian National University, G. P. O. Box 4, Canberra. A. C. T. 2601, Australia

ABSTRACT A mechanism by which NH stretching quanta are coherently transported along a chain of hydrogen bonded peptide groups is demonstrated by classical simulation of a section of the α-helical peptide poly(L-alanine). Vibrational motion takes place on a complex energy surface constructed from earlier ab initio and empirical surfaces. A speculative hypothesis of the biological role of this mechanism is presented, and the critical parameters governing the dynamics are identified and discussed.

INTRODUCTION

The mechanisms by which energy is transported between sites of chemical reactivity in membrane-bound proteins are important subjects in current molecular biology. This and two previous papers propose and investigate an interesting mechanism whereby large quanta of vibrational energy may be transported coherently through the network of hydrogen bonds in α-helical proteins.

The first paper in this series (1) dealt with a very simple model of hydrogen bonded amides: sufficiently simple to allow a clear exposition of the mechanism proposed and to allow both analytic and numerical solutions of the classical and quantum dynamics. The mechanism relies on two Fermi resonance interactions: between NH stretching vibrations and Amide-I modes on the same molecule and on the adjacent hydrogen bonded molecule. From this simple model, three main points emerge. First, when the rates of intra and inter molecular energy transfer are approximately equal, coherent energy transfer via a solitonlike pulse occurs. Second, under certain conditions, the classical dynamics of such a chain of coupled oscillators qualitatively reproduces the features of the quantum dynamics of the chain. Third, the Fermi resonance mechanisms produce a group velocity for the energy pulse that is much greater than that expected for optical phonons.

A second paper (2) dealt with a model of chains of hydrogen bonded *N*-methylacetamide (NMA) which occur in the solid state. Using a realistic potential energy surface, classical simulations demonstrated that coherent energy transfer occurs in this system by essentially the same means as in the simple model, despite the presence of many other degrees of freedom in this large molecular aggregate. An energy pulse was found to transfer between molecules on the subpicosecond timescale. These simulations invoked a number of simplifying approximations, including a linear hydrogen bonding geometry and restriction to two dimensional motion. This paper discards many of these approximations.

Here we report simulations which show that coherent energy transport is theoretically possible in a model system whose parameters closely approximate conditions in an α-helical protein. The following section explains, in the context of an unashamedly speculative hypothesis, why such energy transfer could be important in a biological context. The section entitled Mechanism gives a qualitative description of the energy transfer mechanism. The next section contains a brief description of the model peptide, α-Poly(L-alanine). The remaining Sections of the paper are devoted to a demonstration of the energy transfer process. We present a detailed derivation of the potential energy surface constructed to describe the vibrational motion of this peptide; note some essential computational details; and present the results of classical simulations of vibrational energy redistribution after excitation of NH stretching near one end of the helix. These results are discussed and related to earlier work.

ENERGY CONDUCTION IN PROTEINS

The idea that vibrational energy, from the hydrolysis of adenosine triphosphate (ATP), can propagate through the hydrogen bonds of proteins as a localized pulse has been considered previously, albeit via a very different mechanism (3 and references therein). However, this localized excitation has been shown, in classical simulations, to be unstable at temperatures as high as room temperature and to be trapped at low temperature (4).

We propose a new mechanism, based on Fermi resonance processes. However, before exploring this

0006-3495/91/02/316/18 $2.00

mechanism, one should consider the biological context. It is not clear how an α-helical protein could become involved in the transport of vibrational energy created by hydrolysis of ATP, or how a cell might use such a process. We have attempted to examine these questions. The argument developed below is not the result of years of study in biochemistry. However, it is an attempt to weld together parts of the recent knowledge gained about the structure and function of membrane-bound proteins into a feasible, if extremely speculative, hypothesis.

Hopefully, this hypothesis and, perhaps more importantly, a demonstration of the mechanism will provoke further study.

BIOLOGICAL HYPOTHESIS

Many important functions of cells are carried out within and at the surface of membrane-bound proteins. Pertinent examples include the ATPase ion pumps, such as the Na^+/K^+ and Ca^{2+} pumps (5, 6), which maintain ion concentrations within the cell against a concentration gradient. The direct supply of energy to these pumps is provided by the hydrolysis of ATP to adenosine diphosphate (ADP):

$$ATP^{4-} + H_2O \rightarrow ADP^{3-} + HPO_4^{2-} + H^+, \qquad (1)$$

(under normal physiological conditions).

ATP is the common energy currency of the cell, so that its synthesis and hydrolysis are among the most actively studied processes in bioenergetics (7, 8). Nevertheless, the detailed mechanism by which the energy of this exoenergetic hydrolysis is used to accomplish ion transport is not known.

In recent years, the structure of membrane bound proteins has become much more clearly understood. In a very few cases (9, 10) electron microscopy and x-ray diffraction have been used to provide a complete structure. In many other cases, the complete residue sequence is known, and together with computational models of protein folding, a fairly accurate picture of the secondary structure can be determined (5, 11, 12). One conclusion from these studies has been that interlocking α-helices almost certainly comprise the predominant secondary structure in the membrane spanning regions of such proteins (12). These helices typically span the membrane, a distance of ~30 Å, requiring each helix to be at least 20 peptide units in length. The function of such bundles of α-helices is by no means completely understood, though there is evidence that ion channels are formed within them (13, 14), and site directed mutagenesis can be used to indicate the function of particular residues (6, 14).

It is known that the hydrolysis of ATP takes place while it is bound (as a magnesium complex) to the inner surface of such membrane-bound proteins. No definitive structure for these binding sites is available at present. However, two similar models have been proposed in recent years (15, 16) which are based on folding models, an evaluation of the role of residue sequences which are conserved in a number of related proteins, and the effects of mutagenesis directed at these conserved sites. A full account of these models is given in the references above, though it is important to note that such models are continually being refined in the light of recent rapid progress. While acknowledging the danger of oversimplification, we can summarize the situation as follows. The models postulate a role for four conserved residue sequences in binding ATP (denoted sites III to VI [15]). These sites lie at the sides of a binding pocket formed by a postulated succession of β-α-β segments (16). Sites IV, V, and VI are predicted to play a role in binding the nucleotide, sites III and VI to participate in binding the phosphate groups. A short α-helical segment at one end of sequence VI may (15) bind the α phosphate group in similar fashion to that seen in the binding of several soluble proteins with phosphate moieties (17, 18). There, x-ray diffraction studies have shown that phosphate moieties bind strongly to enzymes with a βαβ secondary structure (18). The binding usually involves the formation of a single (or possible two) hydrogen bond between a phosphate oxygen and an NH group at the terminus of the α-helical segment. This is not surprising since the dipole moment of an α-helix is equivalent to a charge of $\sim +\frac{1}{2}$ at the NH terminus (17). Alterations to amino acids in sequences III to VI show (19) inhibited Ca^{2+} transport and dephosphorylation rather than inhibition of ATP binding.

In the ATPase proteins, the γ phosphate group of ATP is thought to lie close to the phosphorylation site (20, 21), an Aspartate residue (Asp^{351} in the Ca^{2+} ATPase of sarcoplasmic reticulum). Mutation of this residue allows hydrolysis but prevents ion transport and so is thought to act as an essential part of the energy transduction process.

We note that this Aspartate lies close in sequence, and possibly close in proximity, to the end of stalk helix 4 (15), one of four helices which span the membrane and have a hydrophilic extension into the cytoplasm. These α-helices are thought to form (15) a membrane-spanning bundle enclosing an ion channel. At some point in this channel, particular residues form the active ion gates and binding sites (13, 14). A recent study has also identified a high affinity metal binding site in the stalk region; a probable location for Ca^{2+} binding (22).

Again, it is interesting to note that the residues near the end of stalk helix 4 are strongly conserved (much more so than the corresponding segments of stalk helices 1–3). Unfortunately, no site directed mutagenesis has been carried out on this sequence, as far as we are aware.

The γ phosphate group is cleaved during the hydrolysis of ATP. In solution, under physiological conditions, the free energy release of this hydrolysis is ~ 9 kcal mol^{-1}. However, the reverse reaction taking place on mitochondria has been estimated (8) to have a ΔG of 17–17.5 kcal mol^{-1}. In other units, the equilibrium free energy released at the protein by the hydrolysis is probably in the range 3,150–6,100 cm^{-1}. Exactly how much energy is released as usable work in the kinetic process of bond cleavage is not known with great certainty. However, it is quite reasonable to expect that somewhere in excess of 3,000 cm^{-1} of vibrational energy is released.

It seems evident that the site of ATP hydrolysis and the ion binding and gate sites are not directly adjacent. By some means, energy must be transferred from the site of hydrolysis to the ion binding or ion gate sites, possibly through the stalk or transmembrane α-helical segments. The NH stretching modes of the protein, $\sim 3{,}300$ cm^{-1}, and the CO stretching and/or NH in-plane bending modes $\sim 1{,}550$–$1{,}650$ cm^{-1}, are very well placed in frequency to accept energy of the magnitude released by hydrolysis of ATP. These modes could provide a medium for energy transduction.

In light of these arguments, we adopt a further working hypothesis: that the hydrolysis of ATP at a membrane-bound ATPase leads initially to the excitation of NH stretching or CO stretching-NH bending modes localized at one terminus of an α-helix.

In the following sections we explore the consequences of vibrationally exciting the protein in this way.

MECHANISM

We have shown previously (2) that crystalline *N*-methylacetamide, which contains the *trans* peptide group, exhibits 2:1 Fermi resonance coupling between the NH stretch and the NH in-plane bending motions contained in the Amide-I and Amide-II modes. It is, therefore, important at this point to understand the qualitative character of these principal vibrational motions (23, 24).

The Amide-I mode [$\approx 1{,}655$ cm^{-1} in poly(L-alanine) or secondary amides in condensed phases] is characterised largely by C=O stretching ($\approx 80\%$ in potential energy distributions) and to a lesser extent NH in-plane wagging ($\approx 10\%$) and CN stretching ($\approx 10\%$). Whereas the NH wagging component is small in potential energy terms, the relatively light mass of the hydrogen means wagging amplitude is still significant. The Amide-II mode ($\approx 1{,}550$ cm^{-1} in condensed phases) involves a large amount of NH in-plane wagging ($\approx 60\%$). This vibration also involves CN stretching ($\approx 40\%$) and some smaller contributions from NC stretching and CO in-plane wagging.

The so called Amide-B band (3,100 cm^{-1}) in the vibrational spectra of secondary amides and polypeptides has been associated with Fermi resonance. In *cis* secondary amides (25) this band has been identified with a Fermi resonance between the NH stretch and the combination of CO stretching and NH bending modes at approximately 1,650 cm^{-1} and 1,450 cm^{-1}, respectively. In *trans* peptides (25–28) this band is generally thought to be the result of a Fermi resonance between the NH stretch and the overtone of the Amide-II mode (*cis* secondary amides do not exhibit an Amide-II mode). A more recent study (29) has considered a manifold of states including the overtone of the Amide-I mode and the third overtone of the NH out-of-plane bend (≈ 780 cm^{-1}) to describe both the Amide-A ($\approx 3{,}280$–$3{,}300$ cm^{-1}) and Amide-B bands at low temperatures. The 2:1 frequency matching needed for resonance with the Amide-A mode is closest to being fulfilled by the Amide-I mode, and it is this mode, rather than the Amide-B mode, which we consider herein.

Whereas there is evidence for Fermi resonance type interactions, (the intensity of the Amide-B band is too great to be the pure overtone of the Amide-II and must contain some NH stretch character), it is certainly not clear that a simple interpretation is appropriate. We have seen that if multiple Fermi resonance interactions exist within and between molecules, the expected Fermi splittings may be diminished and therefore a theoretical analysis in terms of a single resonance or a single molecule would not be accurate. It should also be noted that the overtone of the Amide-I mode corresponds to the middle of the broad Amide-A band so there is little chance of resolving it and determining any Fermi shift.

Hydrogen bonding occurs between NH and CO groups on adjacent amide groups in the condensed state; for example, in crystalline *N*-methylacetamide (30). In the α-helix, three hydrogen bonding chains or spines are set up between peptide groups on adjacent turns, as illustrated in Fig. 1. This hydrogen bonding directly couples modes involving the NH and CO stretching via both harmonic and anharmonic terms in the potential energy. We have shown previously (2) that anharmonic coupling terms proportional to the donor NH bond length displacement and the acceptor C=O bond length displacement squared are likely to be significant in magnitude and in their effect on dynamics.

The special properties of this peptide group comes from the combination of three features: the near 2:1

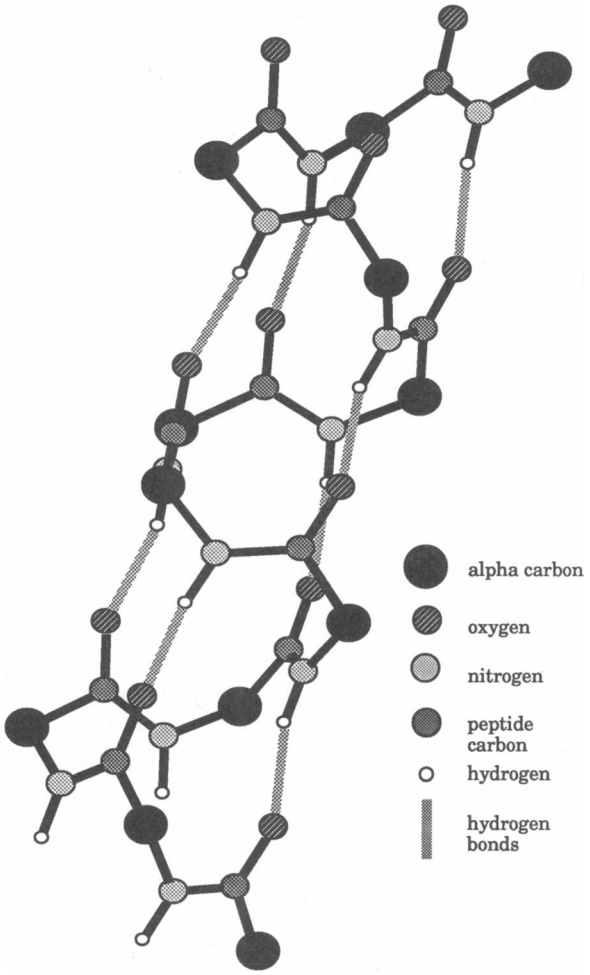

FIGURE 1 A section of α_I-helix. For clarity, substituents on the alpha carbon are not shown.

ratio of the NH stretch and Amide-I frequencies when hydrogen bonding is present, together with the known kinematic coupling of stretching and bending modes (31–33); the involvement of the CO stretch in the Amide-I mode, which, owing to the head to tail arrangement of hydrogen bonding, is directly coupled to the next NH stretch; and the reasonable possibility of suitable cubic coupling terms existing across the hydrogen bond.

The following scenario becomes possible: upon excitation of the NH stretch at $\sim$3,300 cm^{-1}, energy will be transferred into the Amide-I mode (and possibly the Amide-II mode) by an intramolecular (stretch-wag) Fermi resonance and therefore into the CO stretch. This group is hydrogen bonded to the NH on the next peptide group, and is in 2:1 resonance with its stretch. Given suitable anharmonic coupling, energy will be transferred by an intermolecular Fermi resonance into the next molecule, and so on. A concerted flow of energy, by nonlinear resonances, becomes possible along the hydrogen bonded spine of an α-helix. Alternatively, if two quanta of the Amide-I mode were initially excited, energy could flow by the same means.

α-POLY (L-ALANINE)

A generalized α-helix (34, 35) is shown in Fig. 1. The hydrogen bonding pattern has the NH on residue n bonded to the CO on residue $n + 3$. We model α-poly(L-alanine), [α-$(Ala)_n$], whose geometrical parameters (36) (see Table 1) conform very closely to those of the standard α_I- helix. This particular α-helix has been chosen for the simulation because it is the simplest observed α-helix, with only methyl and hydrogen substituents on the α-carbon.

To simplify the dynamics, the methyl substituent is replaced by a point mass. This is done to remove degrees of freedom which are unlikely to be important. We model a section of helix 21 residues long. Therefore, each of the hydrogen bonded chains running down the helix contains seven residues. This length is characteristic of α-helical sections in membrane-bound proteins.

POTENTIAL ENERGY SURFACE

An advantage of specifically modeling α-$(Ala)_n$ is that there is a potential energy surface available using the point mass approximation for the methyl group. This surface of Dwivedi and Krimm (37) (DK), derived from a number of previous surfaces for polypeptides (38 and references therein), has been adopted as a starting point in our investigations. However, there are three areas of difficulty for implementation of the DK surface which require modifications.

TABLE 1 **Geometry of α-Poly(L-alanine)***

Bond lengths		Bond angles		Dihedral angles	
(Å)		(Deg)		(Deg)	
$r(C^{\alpha}C)$	1.53	$\theta(C^{\alpha}CN)$	115.4	$\tau(NC^{\alpha}), \phi$	−57.4
$r(CN)$	1.32	$\theta(CNC^{\alpha})$	120.9	$\tau(C^{\alpha}C), \psi$	−47.5
$r(NC^{\alpha})$	1.47	$\theta(C^{\alpha}CO)$	121.0	$\tau(CN), \omega$	180.0
$r(CO)$	1.24	$\theta(CNH)$	123.0		
$r(C^{\alpha}H)$	1.07	$\theta(NC^{\alpha}Me)$	109.9		
$r(NH)$	1.09	$\theta(CC^{\alpha}Me)$	109.5		
$r(C^{\alpha}Me)$	1.53	$\theta(NC^{\alpha}H^{\alpha})$	109.5		
		$\theta(CC^{\alpha}H^{\alpha})$	109.5		
$r(NO)$	2.86	$\theta(NHO)$	164.2		
$r(OH)$	1.88	$\theta(HOC)$	156.2		

*Reference 35.

The first difficulty is the choice of coordinates. The DK potential surface is expressed in a set of redundant coordinates. A 21-residue section of helix contains 147 particles so there need only be 435 nonredundant coordinates, but 885 internal coordinates are used to calculate the energy. Thus, the force constants are not partial derivatives of the energy. This restricts comparison of these force constants with those of other surfaces, and inhibits improvement of the surface. Furthermore, the dihedral angles across the hydrogen bonds, R_{28} and R_{29} (see Table 2) are poor choices of dynamical coordinates because the NHO and HOC angles are so close to 180°. These coordinates have very small diagonal force constants (0.0005 aJ for τ_{NH} and 0.001 aJ for τ_{CO}), no off diagonal terms, and the rigidity of the backbone of the α-helix should ensure that the coordinates are restrained, so these terms in the DK surface are discarded. Removing these coordinates does not have significant effect on the calculated vibrational frequencies.

The second problem with implementation of the potential energy surface is that Dwivedi and Krimm (37) calculate the frequency dispersion for the Amide-I and Amide-II modes using transition dipole coupling (39) (TDC) perturbatively. This cannot be reproduced in dynamics. Moreover, it is difficult to formulate a satisfactory framework to accurately include the most important electrostatic couplings by this means, as the dipole–dipole approximation is inadequate at the short separation of neighboring groups. These interactions have been discarded and partially replaced by cross-hydrogen bond intermolecular force constants calculated by evaluating the second derivatives of the intermolecular potential of Jorgensen and Swenson (40), for two peptide groups set up in the helix hydrogen bonding geometry, in terms of a complete set of internal coordinates. The significant interpeptide force constants are given in Table 3. All the intrapeptide terms thus calculated were discarded as it would be inappropriate to include these in addition to the DK intrapeptide force constants. The force constants of Table 3 involving r_{OH}, θ_{NHO} and θ_{HOC} replace those of the DK surface.

The final and most important difficulty concerns the general quality of the force field. The intrapeptide part of the DK potential is compared, in Table 4, to the intramolecular parts of three NMA ab initio force fields (41–43) and to the intramolecular part of our (2) NMA chain potential, all recast in the internal coordinates of the helix. One should keep in mind the different conditions under which these force fields have been derived. Nevertheless, a fairly obvious conclusion can be drawn from Table 4. Clearly, the four NMA force fields bear a stronger resemblance to each other than to the DK surface. The major distinguishing feature of the DK surface is that it neglects a large number of off-diagonal terms. Whereas a transferrable, semi-empirical, force field could not include every possible coupling, a reason-

TABLE 2 Internal coordinates for α-Poly(L-alanine)*

$R_1 = \Delta r(C^{\alpha}C)$	$C^{\alpha}C$ stretch	$R_2 = \Delta r(CN)$	CN stretch
$R_3 = \Delta r(NC^{\alpha})$	NC^{α} stretch	$R_4 = \Delta r(CO)$	CO stretch
$R_5 = \Delta r(NH)$	NH stretch	$R_6 = \Delta r(C^{\alpha}H^{\alpha})$	$C^{\alpha}H^{\alpha}$ stretch
$R_7 = \Delta r(C^{\alpha}Me)$	$C^{\alpha}Me$ stretch	$R_8 = \Delta r(OH)$	O···H stretch
$R_9 = \Delta\theta(C^{\alpha}CN)$	$C^{\alpha}CN$ ang bend	$R_{10} = \Delta\theta(CNC^{\alpha})$	CNC^{α} ang bend
$R_{11} = \Delta\theta(NC^{\alpha}C)$	$NC^{\alpha}C$ ang bend	$R_{12} = \Delta\theta(C^{\alpha}CO)$	$C^{\alpha}CO$ ang bend
$R_{13} = \Delta\theta(NCO)$	NCO ang bend	$R_{14} = \Delta\theta(CNH)$	CNH ang bend
$R_{15} = \Delta\theta(C^{\alpha}NH)$	$C^{\alpha}NH$ ang bend	$R_{16} = \Delta\theta(NC^{\alpha}H^{\alpha})$	$NC^{\alpha}H^{\alpha}$ ang bend
$R_{17} = \Delta\theta(NC^{\alpha}Me)$	$NC^{\alpha}Me$ ang bend	$R_{18} = \Delta\theta(CC^{\alpha}H^{\alpha})$	$CC^{\alpha}H^{\alpha}$ ang bend
$R_{19} = \Delta\theta(CC^{\alpha}Me)$	$CC^{\alpha}Me$ ang bend	$R_{20} = \Delta\theta(H^{\alpha}C^{\alpha}Me)$	$H^{\alpha}C^{\alpha}Me$ ang bend
$R_{21} = \Delta\theta(HOC)$	H···OC ang bend	$R_{22} = \Delta\theta(NHO)$	NH···O ang bend
$R_{23} = \Delta\omega(CO)$	CO out of plane deformation	$R_{24} = \Delta\omega(NH)$	NH out of plane deformation
$R_{25} = \Delta\tau(C^{\alpha}C)$	$C^{\alpha}C$ torsion	$R_{26} = \Delta\tau(CN)$	CN torsion
$R_{27} = \Delta\tau(NC^{\alpha})$	NC^{α} torsion	$R_{28} = \Delta\tau(CO)$	CO torsion
$R_{29} = \Delta\tau(NH)$	NH torsion		
$T_1 = R_{1D}$	$T_2 = R_{2D}$	$T_3 = R_{3D}$	$T_4 = R_{4D}$
$T_5 = R_{5D}$	$T_6 = R_{1A}$	$T_7 = R_{2A}$	$T_8 = R_{3A}$
$T_9 = R_{4A}$	$T_{10} = R_{5A}$	$T_{11} = R_8$	$T_{12} = R_{9D}$
$T_{13} = R_{10D}$	$T_{14} = R_{13D}$	$T_{15} = R_{14D}$	$T_{16} = R_{9A}$
$T_{17} = R_{10A}$	$T_{18} = R_{12A}$	$T_{19} = R_{14A}$	$T_{20} = R_{21}$
$T_{21} = R_{22}$			

*See reference 37 for full definition of out of plane deformations and torsional coordinates. Coordinates T_i are used to describe the cross-hydrogen bond potential energy, where A and D denote coordinates on donor and acceptor molecules in the hydrogen bond, respectively.

TABLE 3 **Interpeptide force constants***

Coordinates T_iT_j	Force constant	Coordinates T_iT_j	Force constant	Coordinates T_iT_j	Force constant	Coordinates T_iT_j	Force constant
11,11	0.166	20,8	0.001	20,20	0.000	20,10	0.002
21,21	0.049	20,16	0.005	11,21	0.055	20,17	0.003
20,21	0.011	20,18	0.006	11,1	0.003	2,9	0.003
11,2	0.012	2,16	0.001	11,4	0.004	2,18	0.001
11,5	0.270	3,9	0.001	11,8	0.002	5,16	0.004
11,9	0.012	5,18	0.003	11,10	0.003	12,16	0.001
11,12	0.025	14,16	0.001	11,14	0.002	14,18	0.001
11,15	0.028	15,9	0.002	11,16	0.006	15,16	0.003
11,17	0.001	11,18	0.005	11,19	0.001	21,1	0.002
21,2	0.012	21,4	0.002	21,5	0.045	21,7	0.001
21,12	0.018	21,15	0.018	21,17	0.003		

*Units: stretching, aJ/Å^2; bending aJ; bend stretch coupling aJ/Å.

able number of these neglected couplings are relatively large in all the other force fields, (see for example the $r_{C_\alpha N}$, θ_{CNH} or r_{CN}, $\theta_{C_\alpha NH}$ terms).

The large differences in off-diagonal force constants do not affect the frequency spectrum as much as the character of the normal modes. In particular, for the DK surface, the Amide-I modes show a negligible involvement of the NH wagging motion by comparison with all the other surfaces. This is surprising, because it is generally expected that the intra-peptide dynamics of the helix would be similar to that of NMA; indeed this has been the justification for the general interest in NMA. Consequently, the intrapeptide part of the DK helix potential energy surface was replaced by the intramolecular part of our NMA surface (2) (Table 4).

The resultant hybrid force field produced Amide-I and Amide-II frequencies for the helix and the *N*-deuterated helix that are within 25 cm^{-1} of the experimental values (44). However, the errors combine to give frequency shifts on deuteration that are significantly higher than reported. Whereas this seems to indicate an excessive amount of the NH wag in the Amide-I and Amide-II modes, it is dangerous to relate the deuterated frequency shift totally to the amount of NH(D) wag character in the mode; to do so assumes the character of the mode does not change upon deuteration. Moreover, the spectroscopy of α-(Ala)$_n$ suffers from similar uncertainty (45, 46) to that evident for NMA (2). In particular, there must be some doubt over the resolution of small deuteration frequency shifts, in relatively broad bands, for only partially deuterated samples (44). For example, the Amide-I deuteration frequency shifts observed by Rabolt et al. (44) are only 3 and 8 cm^{-1} for Raman and infrared, respectively, whereas the Amide-I bands have a FWHM of the order of 30 cm^{-1} for the Raman and 100 cm^{-1} for the infrared spectrum. The undeuterated component of these samples dominates the spectrum.

To attempt to correct for these discrepancies, a very simple refinement procedure was used to scale the diagonal force constants of the r_{CO}, r_{CN} stretch and the θ_{CNH} and $\theta_{C_\alpha NH}$ in-plane wag coordinates, those principally involved in the Amide-I, II vibrations, to provide better agreement with experiment. The average of the middle 19 of the 21 frequencies for each mode was taken to give the theoretical frequency to avoid problems with modes lying at the ends of the helix, and the four force constants were scaled by no more than 10%. The scaling procedure was otherwise the same as that used for NMA (2, 47).

Scaling could not reduce the Amide-I deuteration frequency shift below 21.5 cm^{-1} without allowing extraordinarily low values for some force constants. Owing to the importance of this mode, two sets of scaled force constants are examined with deuterated shift of 21.5 cm^{-1}, P1, and the other 25.9 cm^{-1}, P2. The final value of the deuterated frequency shift is still 13 cm^{-1} higher than that seen in one experiment. The final frequencies obtained in the two scaling runs are given in Table 5, along with the frequencies to which they were fitted. The final (2, 2), (4, 4), (14, 14) and (15, 15) force constants of Table 4 are then, respectively, 6.913, 10.000, 0.448 and 0.392 for P1 and 6.770, 9.938, 0.459 and 0.393 for P2.

The final form of the potential surface has thus become a sum over residues or peptide groups of the form:

$$V = \sum_{n=1}^{21} [V_{intra}(n) + V_{RDK}(n) + \sum_{n=1}^{18} [V_{inter}(n, n+3) + V_{anh}(n, n+3)] \quad (2)$$

TABLE 4 Comparison of the intra-peptide force constants*

Coordinate R_iR_j	Description	Dwivedi and Krimm‡	Balazs§	Sugawara et al., 1984‖	Sugawara et al., 1986¶	Clarke and Collins**
1,1	$C^{\alpha}C$	4.160	4.321	4.760	5.000	3.676
2,2	CN	6.415	6.630	7.750	8.110	6.791
3,3	NC^{α}	4.823	5.260	5.350	6.020	5.521
4,4	CO	10.029	11.750	10.020	13.200	9.802
5,5	NH	5.830	6.718	0.000	8.230	0.000
9,9	$C^{\alpha}CN$	0.833	0.924	0.940	0.860	0.643
10,10	CNC^{α}	0.826	1.131	0.560	0.727	0.593
12,12	$C^{\alpha}CO$	1.046	0.924	0.681	0.841	0.566
13,13	NCO	1.446	1.709	0.889	1.049	0.672
14,14	CNH	0.556	0.561	0.447	0.544	0.498
15,15	$C^{\alpha}NH$	0.556	0.561	0.413	0.509	0.436
1,2	$C^{\alpha}C$, CN	0.300	0.294	0.350	0.350	0.274
1,3	$C^{\alpha}C$, NC^{α}	0.100	−0.026	−0.030	−0.030	−0.025
1,4	$C^{\alpha}C$, CO	0.500	0.404	0.520	0.520	0.340
1,5	$C^{\alpha}C$, NH	0.000	0.007	0.000	0.020	0.004
1,9	$C^{\alpha}C$, $C^{\alpha}CN$	0.300	0.057	0.204	0.204	−0.083
1,10	$C^{\alpha}C$, CNC^{α}	0.000	0.034	0.008	0.008	0.026
1,12	$C^{\alpha}C$, $C^{\alpha}CO$	0.100	−0.057	0.117	0.117	−0.141
1,13	$C^{\alpha}C$, NCO	0.000	0.390	−0.321	−0.321	0.224
1,14	$C^{\alpha}C$, CNH	0.000	0.020	0.010	0.010	−0.005
1,15	$C^{\alpha}C$, $C^{\alpha}NH$	0.000	−0.020	−0.018	−0.018	−0.021
2,3	CN, NC^{α}	0.300	0.098	0.230	0.230	0.101
2,4	CN, CO	0.500	1.247	1.520	1.520	1.154
2,5	CN, NH	0.000	0.002	0.000	0.010	0.023
2,9	CN, $C^{\alpha}CN$	0.300	0.323	0.098	0.098	0.138
2,10	CN, CNC^{α}	0.600	0.178	0.245	0.245	0.107
2,12	CN, $C^{\alpha}CO$	0.000	−0.323	−0.452	−0.452	−0.339
2,13	CN, NCO	0.200	0.353	0.354	0.354	0.201
2,14	CN, CNH	0.294	0.183	0.047	0.047	0.110
2,15	CN, $C^{\alpha}NH$	0.000	−0.183	−0.292	−0.292	−0.217
3,4	NC^{α}, CO	0.000	−0.056	−0.060	−0.060	−0.052
3,5	NC^{α}, NH	0.000	−0.039	0.000	−0.020	−0.039
3,9	NC^{α}, $C^{\alpha}CN$	0.000	0.017	0.041	0.041	0.058
3,10	NC^{α}, CNC^{α}	0.150	0.246	0.253	0.253	0.178
3,12	NC^{α}, $C^{\alpha}CO$	0.000	−0.017	0.015	0.015	0.031
3,13	NC^{α}, NCO	0.000	−0.139	−0.056	−0.056	−0.089
3,14	NC^{α}, CNH	0.000	−0.185	−0.275	−0.275	−0.227
3,15	NC^{α}, $C^{\alpha}NH$	0.294	0.185	0.022	0.022	0.049
4,5	CO, NH	0.000	−0.024	0.000	−0.060	−0.018
4,9	CO, $C^{\alpha}CN$	0.150	−0.354	−0.498	−0.498	−0.340
4,10	CO, CNC^{α}	0.000	−0.031	0.008	0.008	−0.022
4,12	CO, $C^{\alpha}CO$	0.450	0.354	0.171	0.171	0.103
4,13	CO, NCO	0.450	0.409	0.327	0.327	0.236
4,14	CO, CNH	0.000	0.045	0.031	0.031	0.042
4,15	CO, $C^{\alpha}NH$	0.000	−0.045	−0.039	−0.039	−0.020
5,9	NH, $C^{\alpha}CN$	0.000	−0.025	0.000	−0.041	−0.015
5,10	NH, CNC^{α}	0.000	−0.121	0.000	−0.073	−0.107
5,12	NH, $C^{\alpha}CO$	0.000	0.025	0.000	−0.001	−0.019
5,13	NH, NCO	0.000	0.073	0.000	0.042	0.034
5,14	NH, CNH	0.000	0.031	0.000	0.058	0.109
5,15	NH, $C^{\alpha}NH$	0.000	−0.031	0.000	0.016	0.005
9,10	$C^{\alpha}CN$, CNC^{α}	0.000	0.062	0.013	0.013	0.035
9,12	$C^{\alpha}CN$, $C^{\alpha}CO$	0.000	−0.924	−0.366	−0.326	−0.269
9,13	$C^{\alpha}CN$, NCO	0.000	−0.017	−0.574	−0.534	−0.374
9,14	$C^{\alpha}CN$, CNH	0.200	0.005	−0.018	−0.018	0.003
9,15	$C^{\alpha}NH$, $C^{\alpha}CN$	0.000	−0.005	0.005	0.005	−0.038

TABLE 4 (continued)

Coordinate R_iR_j	Description	Dwivedi and Krimm‡	Balazs§	Sugawara et al., 1984‖	Sugawara et al., 1986¶	Clarke and Collins**
10,12	CNC^{α}, $C^{\alpha}CO$	0.000	−0.062	−0.041	−0.041	0.007
10,13	CNC^{α}, NCO	0.000	−0.119	0.028	0.028	−0.042
10,14	CNC^{α}, CNH	0.000	−0.014	−0.297	−0.381	−0.328
10,15	CNC^{α}, $C^{\alpha}NH$	−0.040	0.014	−0.263	−0.346	−0.265
12,13	$C^{\alpha}CO$, NCO	0.000	0.017	−0.315	−0.515	−0.297
12,14	$C^{\alpha}CO$, CNH	0.000	−0.005	−0.009	−0.008	−0.038
12,15	$C^{\alpha}CO$, $C^{\alpha}NH$	0.000	0.005	0.050	0.050	0.031
13,14	NCO, CNH	0.251	0.073	0.027	0.027	0.035
13,15	NCO, $C^{\alpha}NH$	0.000	−0.073	−0.055	−0.055	0.006
14,15	CNH, $C^{\alpha}NH$	0.038	−0.561	−0.150	−0.163	−0.170

*Units: stretching, aJ/Å^2; bending aJ; bend stretch coupling aJ/Å. ‡Reference 37; §reference 43; ‖reference 41; ¶reference 42; and **reference 2.

where V_{intra} represents the scaled intrapeptide potential terms given in Table 4 and above; V_{RDK} are the remaining terms from the DK potential surface, given in Table 6; V_{inter} represents the cross-hydrogen bond terms given in Table 3, and V_{anh} is the same cross-hydrogen bond cubic term involving c_{NHCO} for the NMA surface:

$$V_{anh}(n, n+3) = c_{NHCO} T_5(n) T_9^2(n+3), \quad (3)$$

where T_5 is the NH stretch on the donor and T_9 is the CO stretch on the acceptor in the hydrogen bond (see Table 2).

Two very small force constants involving the CO and the NH out of plane deformations with the CN torsion were discarded from the DK surface, without observable distortion of the surface. The small off-diagonal force constants coupling the $r_{NC\alpha}$ and $\theta_{CC\alpha Me}$, and $\theta_{NC\alpha C}$ and $\theta_{C\alpha NH}$ coordinates, which have the values of 0.2 aJ Å^{-1} and −0.1 aJ, respectively in the DK surface, have been set to zero in our force field. Because the C_α and Me atoms have no significant motion in the Amide-I mode, neglect of these terms is unlikely to have significant impact on the dynamics reported. These force constants are only relevant to the low frequency modes which we have not attempted to refine.

TABLE 5 **Refinement of Amide-I and II frequencies (in cm^{-1}) for the potential surfaces**

	Unscaled surface	P_1 surface		P_2 surface	
		Target*	Final	Target*	Final
Amide-I	1668.0	1675.5	1658	1657.5	1657.9
Amide-I-Nd	1624.8	1637.5	1636.5	1632.5	1632.0
Amide-II	1563.4	1544.0	1547.1	1544.0	1544.3
Amide-II-Nd	1474.0	1473.5	1471.4	—	1465.0

*Target frequencies discussed in text.

The set of vibrational frequencies for the potential energy surface P2 is shown as a histogram in Fig. 2, compared to experimental infrared and Raman frequencies. The frequencies were calculated for the complete 21 residue section. Any more direct comparison is difficult, especially below 1,300 cm^{-1}, owing to the congestion of frequencies. From this figure, the generally good agreement of the model vibrational frequencies with the experimental frequencies for α-(Ala-N-H)$_n$ can be seen.

Some problems do remain with this surface. The most significant question concerns the amount of NH bend in the Amide-I modes. It is reasonable to expect the intramolecular part of the force field of NMA to provide a good model for this part of an α-helix, and even though it is likely that the deuterated frequency shift is overestimated, this surface is still considered to be a better representation of the Amide-I mode than that provided by the DK surface. However, it is clear that if the original DK surface is correct, coherent energy transfer via the proposed mechanism is remote. Also, little attention has been placed on the accuracy of the potential in reproducing the vibrational frequencies below ~1,000 cm^{-1}. In the present circumstance, these modes are not expected to have much effect on the dynamics, but this would not necessarily be the case where this potential may be used.

The NH stretching modes have been treated effectively as harmonic oscillators, following the NMA study (2). Morse oscillators were found to be inappropriate in a classical simulation involving transitions only between the ground and first excited state: in this energy region,

TABLE 6 **Force constants for α-Poly(L-anine) in addition to Table 3***

Coordinates R_iR_j	Force constant	Coordinates R_iR_j	Force constant	Coordinates R_iR_j	Force constant	Coordinates R_iR_j	Force constant
6,6	4.523	7,16	0.079	7,7	5.080	7,17	0.317
11,11	1.093	7,18	0.079	16,16	0.765	7,19	0.417
17,17	1.093	7,20	0.415	18,18	0.654	9,11	0.160
19,19	0.981	10,16	0.100	20,20	0.664	11,15	0.000‡
23,23	0.657	11,16	−0.0317	24,24	0.129	11,17	0.200
25,25	0.060	11,19	−0.041	26,26	0.680	11,23	−0.073
27,27	0.087	11,24	0.160	28,28	0.000	29,29	0.000
15,16	0.100	12,18	0.150	16,18	0.019	1,7	0.101
16,20	0.043	1,11	0.300	16,22	0.1022	1,16	0.026
17,19	−0.041	1,18	0.305	17,20	−0.031	1,19	0.367
17,24	0.120	1,20	0.079	18,23	−0.100	3,7	0.101
19,20	−0.031	3,11	0.300	19,23	−0.050	3,16	0.427
22,24	0.007	3,18	0.026	23,24	−0.050	3,17	0.217
23,26	0.000‡	3,19	0.000‡	24,26	0.000‡	3,20	0.079

From reference 38 except where noted with ‡ (see text). Units: stretching, aJ/Å^2; bending aJ; bend stretch coupling aJ/Å.

the NH stretch should be in resonance with a single frequency corresponding to the 0→1 energy gap, whereas a classical Morse oscillator vibrates with a spectrum of frequencies depending on its energy. Moreover, if one considers a first-order time-dependent perturbation treatment of quantum 2:1 Fermi resonance coupling between a Morse oscillator and a harmonic oscillator, it is clear that the transfer rate will depend on Morse matrix elements such as $<\nu = 1|\delta r|\nu = 0>$. Mortenson et al. (48) have shown that for Morse oscillators with relative anharmonicity $\omega/(\omega_e x_e)$ of typically ~50, the harmonic approximation to such matrix elements is in error by only ~3%. Hence, it can be expected that a classical harmonic oscillator simulates a quantum Morse oscillator, in resonance with other modes at low energy, more accurately than does a classical Morse oscillator. For computational convenience, NH oscillators have been described by Morse functions with negligible anharmonicity. For example, an NH frequency ω_{NH} of 3,304 cm^{-1} is given by Morse parameters (2) of D = 9.451 fJ and α = 0.1011 Å^{-1}. Other values of ω_{NH} reported here correspond to the same small relative anharmonicity.

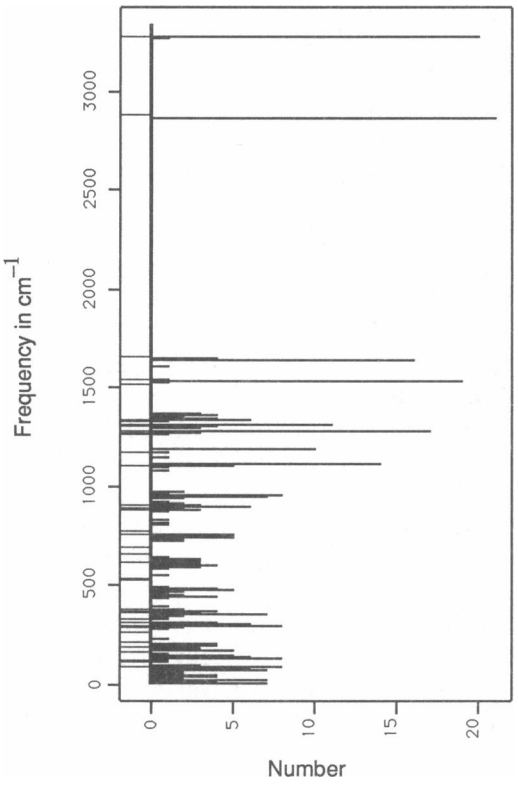

FIGURE 2 Histogram of calculated vibrational frequencies of α-Poly (L-alanine) using the P2 surface, compared to observed (44) frequencies (shown below zero). The bin size is 7.5 cm^{-1}.

COMPUTATIONAL DETAILS

The computational method follows very closely that for the simulation of NMA (2). Trajectories are evaluated in Cartesian coordinates, using the Verlet leap-frog algorithm. Calculations were performed in reduced units, with mass in amu, length in Angstroms, and unit time of 9.552 fs (about one NH stretch period). The unit of energy is then 5.495 aJ (≈9,160 cm^{-1}). Energy was conserved to within 10^{-4} reduced energy units using a time step of 0.02 time units. The trajectories were performed for seven helices simultaneously, requiring ~5 s/(1,000 time steps) per trajectory on a Fujitsu FACOM VP-100.

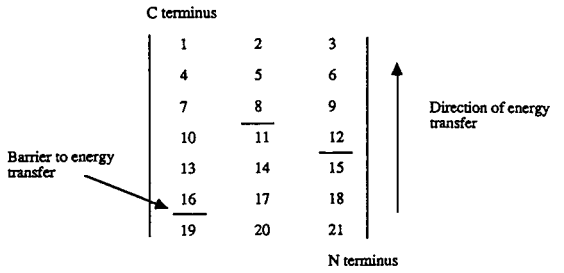

FIGURE 3 The numbering scheme used for a 21-residue section of α-helix. The NH bonds on residues 16,12, and 8 are excited in some simulations reported, with c_{NHCO} set to zero to prevent energy transfer to residues 19,15, and 11.

The α-$(Ala)_n$ helices were set up in the geometry of Table 1. Fig. 3 indicates the numbering scheme of the residues. Residue n is the donor molecule in the hydrogen bond with residue $n + 3$ and the acceptor in the hydrogen bond with residue $n - 3$. The initial excitation was placed in NH oscillators (2). Reduced zero point energy (quasicallical quantum number $v = -0.49$) was used for the Cartesian normal modes and unexcited NH oscillators, to mimic the quantum dynamics more closely (1, 2).

For trajectories where there was only limited energy transfer, it was possible to simultaneously perform three simulations of energy transfer within the 21 residue section of α-helix, as shown schematically in Fig. 3. Three excitations were located on nonneighboring residues to allow three essentially independent simulations of energy redistribution over the three distinct hydrogen bonded chains. This reduces possible bias due to the position of the excitation and improves the statistics. The coupling c_{NHCO} was set to zero for these oscillators so that energy could be transferred only in one direction along the hydrogen bonded chain. When conditions conducive to more coherent energy transfer were employed, single excitations were followed down the complete helix.

A stable method for calculation of the dihedral angles (and their Cartesian derivatives) is required. The dihedral angle τ_{ABCD} is defined to be the angle from the plane containing atoms A, B, C to the plane containing B, C, D in an anticlockwise direction. For bond vectors **a** (B→A), **b** (C→B), and **c** (D→C), a stable description is given by

$$\tau = \arcsin\left[\frac{\mathbf{b}\cdot(\mathbf{a}\times\mathbf{b})\times(\mathbf{b}\times\mathbf{c})}{|\mathbf{b}|\,|\mathbf{a}\times\mathbf{b}|\,|\mathbf{b}\times\mathbf{c}|}\right] + \pi, \qquad (4)$$

for dihedral angles near π, whereas related formulas apply elsewhere.

RESULTS

Three time dependent quantities are reported. The energy of each individual residue or peptide group is approximated by summing the intrapeptide terms, the remaining DK terms, half of the cross-hydrogen bond terms, and the atomic kinetic energy. For simplicity, the energy involved in the motion of C_α and its substituents is included with the peptide group of the adjacent nitrogen. The NH stretch energies (2) and total energies in the Amide-I and II modes are also reported. These quantities were averaged over an ensemble (usually 28) of parallel trajectories and, where applicable, over multiple simulations within the same section of helix.

The NH stretch oscillator frequency and c_{NHCO} were examined to locate the regions of greatest energy transfer for the P1 surface. For the same conditions, trajectories were performed using the P2 surface to investigate the effect of increasing the NH wag character of the Amide-I mode at the optimal conditions.

No anharmonic coupling

Fig. 4 shows the 14 trajectory average energy redistribution following initial excitation of a NH stretch oscillator, without any anharmonic potential coupling ($c_{NHCO} = 0$). An energy of 4,920 cm^{-1} (0.54 energy units) has been placed in the NH oscillator of residue 20 (see Fig. 3). This energy, approximately one quanta above the ground state, was used in all the trajectories with single quanta NH excitations.

An NH frequency of 3,304 cm^{-1} was found to give the fastest overall intramolecular energy transfer: the NH stretch energy reaches a minimum of <5% of the initial excitation at ~0.5–0.6 ps. The familiar stretch-wag Fermi resonance between the NH stretch and the Amide-I mode is clearly reproduced here. Twice the Amide-I frequency is ~3,316 cm^{-1} which, allowing for some anharmonicity in the Amide-I modes, means that the NH stretch frequency of 3,304 cm^{-1} must be very close to the overtone. The Amide-II mode is seen to take a much smaller role in the initial stages of the energy redistribution.

Energy moves much more slowly out of the initially excited molecule, mainly in one direction along the helix backbone to residue 19 (Fig. 5 *b*). This is, perhaps artificially, due to the allocation of the C_α group energy. The timescale is so much slower than the intrapeptide Fermi resonance, that backbone transfer is unlikely to be important. (In fact, when anharmonic coupling is included, >90% of the energy remains in the initially excited hydrogen bonded spine; this percentage may be

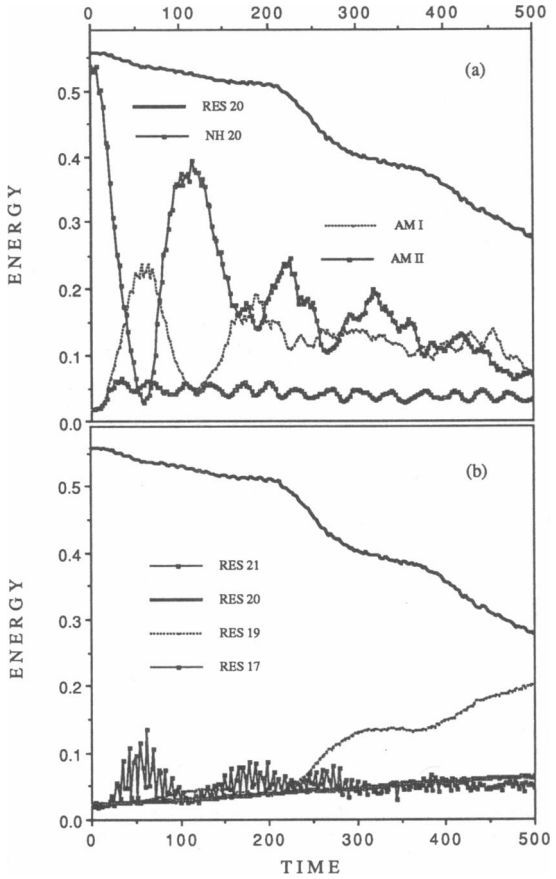

FIGURE 4 Average energy versus reduced time for $c_{NHCO} = 0$ and a NH stretch frequency (ω_{NH}) of 3,304 cm^{-1}: (*a*) total energy for residue 20 and its NH oscillator, and all Amide-I and Amide-II modes; (*b*) the energies of neighbouring residues. Unit time ≈ 1 NH stretch period; unit energy ≈ 9,160 cm^{-1}.

even larger but for the allocation of the C_α energy). We note that the variation in the energy of residue 21 correlates strongly with the energy of the Amide-I mode, indicating that dephasing of the Amide-I modes will be part of this slow energy transfer pathway.

Variation of energy transfer with NH stretch frequency

Preliminary trajectories indicated the range of frequencies and c_{NHCO} couplings that were of interest, so more detailed investigations were performed with NH stretch oscillators whose frequency ranged from 3,338 cm^{-1} to 3,278 cm^{-1} with c_{NHCO} held constant at −4.0 aJ $Å^{-3}$. The results for a frequency of 3,278 cm^{-1} and the optimal frequency of 3,304 cm^{-1} are shown in Figs. 5 and 6. The trajectories were all run for seven helices in parallel using three separate excitations per helix as illustrated in

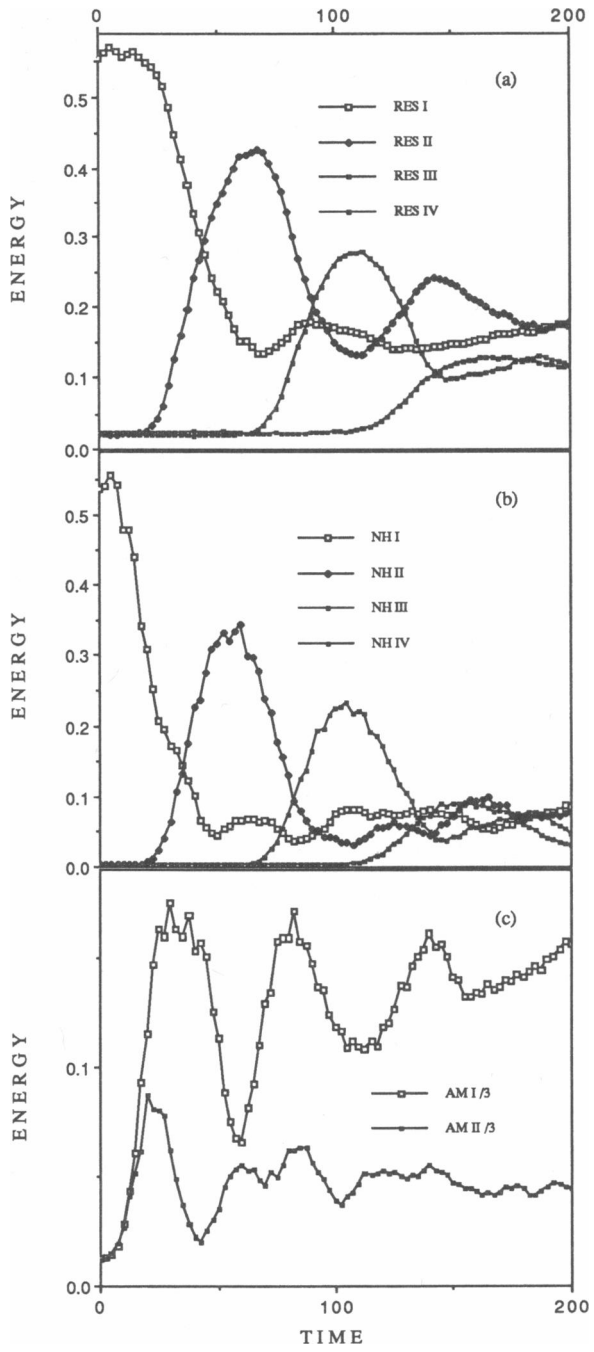

FIGURE 5 Average energy versus time for $c_{NHCO} = -4$ aJ $Å^{-3}$ and ω_{NH} = 3,304 cm^{-1}, where residue I is an average over residues 16, 12, and 8, and so on (see Fig. 3). (*a*) residue energies; (*b*) NH stretch energies for the residues in (*a*); (*c*) average amide mode energies for one excitation.

Fig. 3. The numbering system used in the diagrams has the excitation starting in residue I and proceeding to residue IV. Comparison of the averages for the three separate excitations, within a section of helix, with the

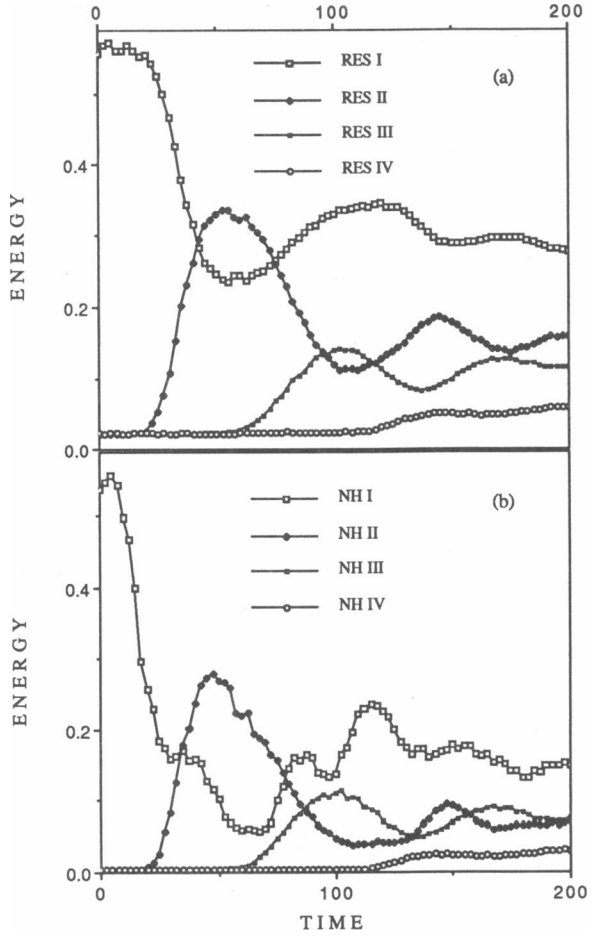

FIGURE 6 As for Fig. 5 (*a*) and (*b*), with ω_{NH} = 3,278 cm^{-1}.

combined averages did not suggest any large excitation-site dependant effects or end effects.

Fig. 5 clearly shows a decaying energy pulse, in both total energy and NH stretch energy, propagating down the hydrogen bonded chain in a very similar manner to that observed previously in NMA simulations (2). The time for the pulse to reach a maximum in the fourth residue in the chain is ~1.5–1.6 ps. However, the energy appears to be partially trapped between the second and third residues, indicating that the cubic potential coupling may be too large.

Changing the NH stretch frequency from 3,304 cm^{-1} up to 3,318 cm^{-1} or down to 3,294 cm^{-1} produced very little observable change in the dynamics. Outside this range the resonance mechanism is strongly perturbed. Fig. 6 shows the effect of a NH frequency of 3,278 cm^{-1}. The energy becomes trapped in the first three residues as the 2:1 frequency matching required for Fermi resonance is poorly satisfied. Similar behavior is observed for a frequency of 3,338 cm^{-1} or higher.

Variation of energy transfer with cubic coupling

With the NH stretch frequency optimised, the cubic potential energy coefficient, c_{NHCO}, was examined. The trajectories of Fig. 5 were repeated with c_{NHCO} of −3.0, −3.5, and −4.5 aJ Å^{-3}. The results for −3.5 are displayed in Fig. 7. Decreasing c_{NHCO} to −3.5 aJ Å^{-3} makes very little change to the transfer timescale or the amount of energy transferred out of the first or second peptide group but the differences are apparent with the third and particularly the fourth peptide group, which gains ~50% more energy. Lowering the cubic coupling term to −3.0 results in slightly less energy transfer, but it is still marginally more efficient than at c_{NHCO} = −4.0 aJ Å^{-3}. Increasing the cubic coupling parameter to −4.5 aJ Å^{-3} leads to less energy leaving the initially excited residue, and only a small amount reaching the fourth.

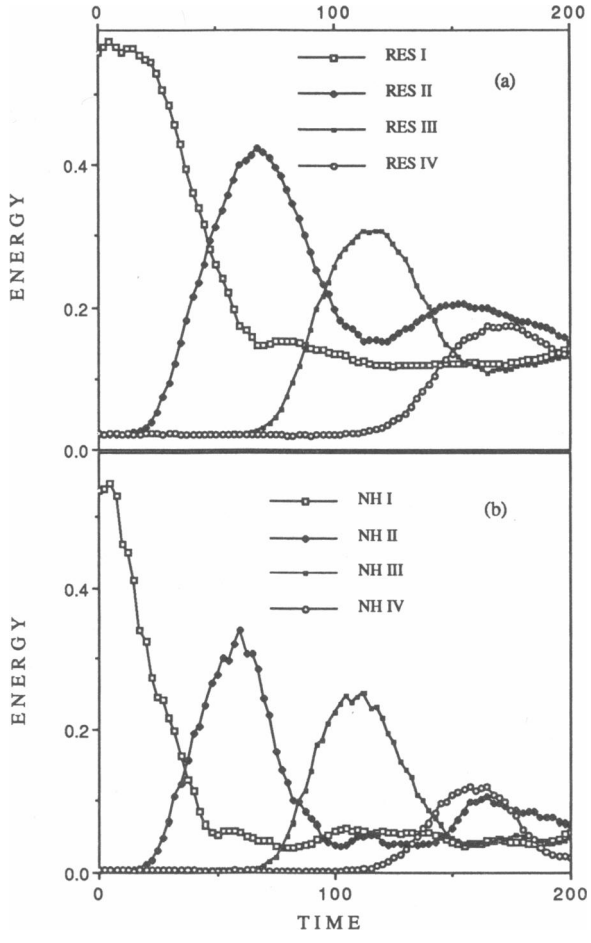

FIGURE 7 As for Fig. 5 (*a*) and (*b*), with c_{NHCO} = −3.5 aJ Å^{-3}.

Longtime simulations at optimal conditions

With the NH stretch frequency and the cubic coupling parameter optimised at 3,304 cm^{-1} and -3.5 aJ $Å^{-3}$ respectively, 28 trajectories were performed over longer time (Fig. 8). The initial excitation was placed in one of the free NH stretch oscillators (residue 20), allowing for energy transfer along the complete hydrogen bonded chain. The energy propagates almost completely down the helix, with a very small amount of energy reaching the seventh residue after about 3.3 ps (350 time units). The coherence of the energy transfer starts to break down after 1.4 ps, when a small secondary pulse is introduced between the second and third residues, which it should be remembered remains after averaging over the trajectories. This apparent disruption of the pulse is probably also a result of the averaging process, as the pulses from each individual trajectory get out of phase further down the molecule. The total Amide-I mode energy, in Fig. 8 *c*, also shows the breakdown of the coherent behavior in the second half of the trajectory.

Increased excitation energy

To investigate the anharmonicity of the system the amount of initial excitation was increased to two quanta above the ground state (8,260 cm^{-1} or 0.90 energy units), keeping all other conditions the same as for Fig. 8. Surprisingly, there is sufficient anharmonicity in the kinetic energy to significantly disrupt the coherent propagation of the energy pulses, so that very little energy reaches beyond residue 11, and the energy propagation is erratic.

P2 surface

The optimal conditions obtained with the standard potential surface, P1, were repeated with the alternative surface, P2, which has enhanced NH wag components of the Amide-I modes. Averages over 28 trajectories are shown in Fig. 9. Comparison of Fig. 9 *a* with Fig. 8 *a* shows a great resemblance up to ~1.4 ps (150 time units), where in Fig. 8 *a*, a small secondary energy pulse develops. In contrast, once the energy pulse has passed a residue in Fig. 9 *a*, the residue does not interact strongly with its neighboring groups even though it still has some energy in it. As a result, the energy pulse is seen to move relatively undisturbed to the end of the helix. The NH energies similarly show the energy pulse moving to the end of the chain. Comparison of the amide mode energies, Figs. 8 *c* and 9 *c*, shows that more energy is observed in the Amide-I modes of Fig. 9 *c* which have greater NH wag component.

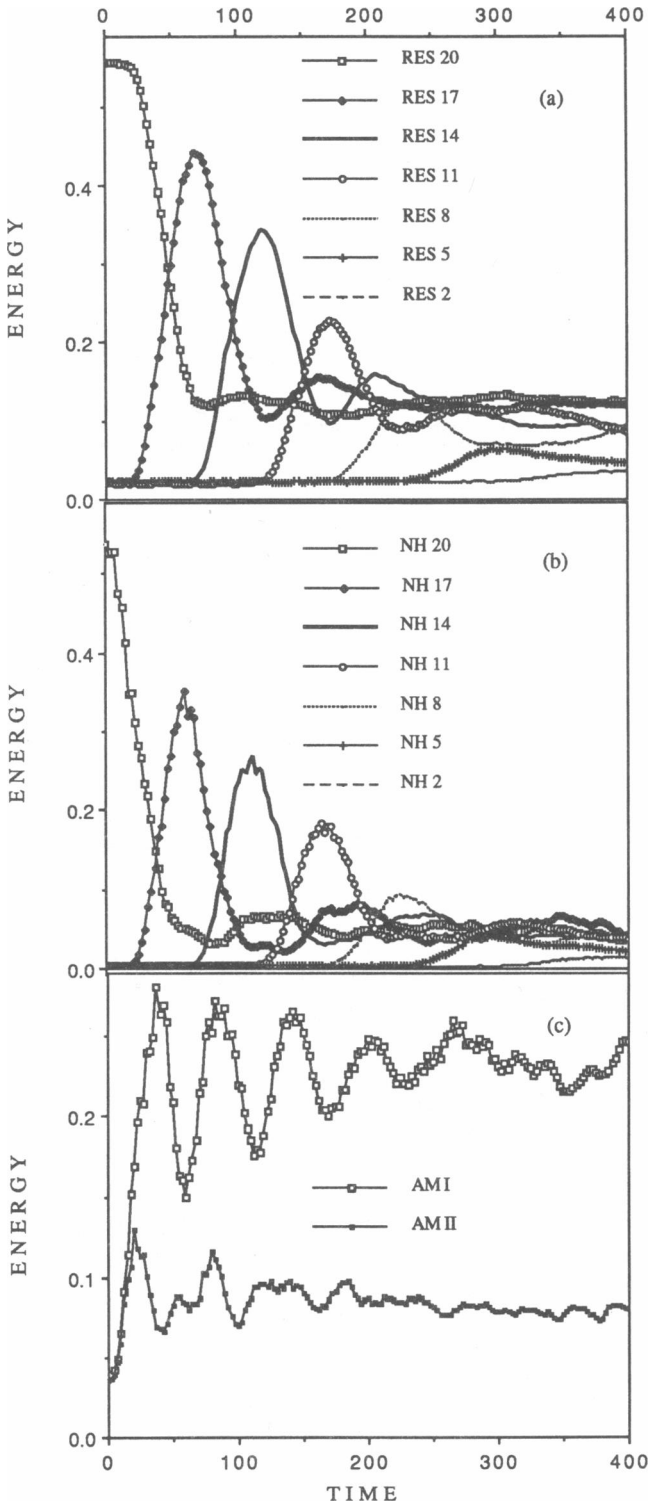

FIGURE 8 Average energy versus time following excitation of the NH stretch on residue 20, for ω_{NH} = 3,304 cm^{-1} and c_{NHCO} = -3.5 aJ $Å^{-3}$: (*a*) residues in the hydrogen bonded chain containing residue 20; (*b*) NH oscillator energies for the residues in (*a*); (*c*) total energy in Amide-I and Amide-II normal modes.

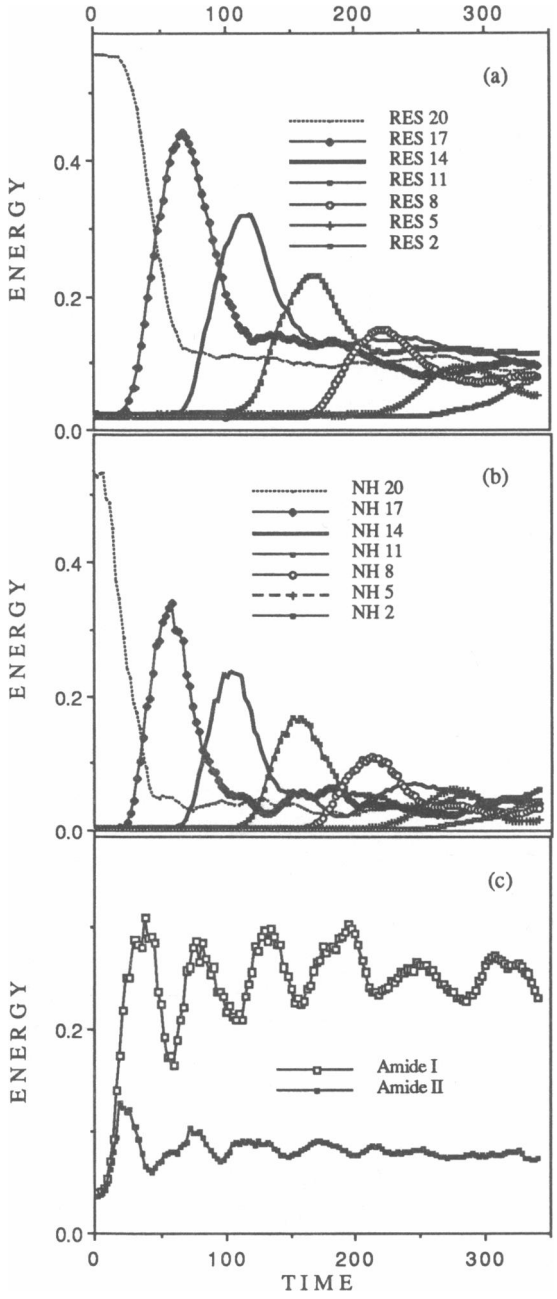

FIGURE 9 As for Fig. 8, using the P_2 surface.

Single trajectories using the P2 surface

Finally we examined a small number of single trajectories that were run at the optimal conditions, using the P2 surface, to exhibit the effects of averaging on the above results. The variation between these single trajectories appeared to be much greater than that seen in NMA simulations (2), where a lower reduced zero-point energy was used. For example, the trajectory displaying the poorest energy transfer diverged from the average behavior (see Fig. 9) after the decay of the initially excited NH stretch at about 75 time units (0.7 ps). Thereafter most of the energy became trapped in the first and second residues. By comparison, Fig. 10 shows a striking example of coherent energy transfer.

From the individual residue energies shown in Fig. 10, a very smooth energy pulse can be clearly seen propagating down the hydrogen bonded chain with, at one time, a maximum energy of approximately half the initial excitation appearing in residue two (that is, about one quanta of Amide-I vibrational energy). This transfer occurs by 350 time units or ~3.3 ps. The proportion of energy transferred from one residue to the next varies from 96 to 87%, whereas the width, as measured by FWHM, only increases from about 0.5 ps for residue 17 to ~0.6 ps for residue five.

The NH stretch energies in Fig. 10 are seen to return to near zero after the pulse has passed, indicating that the small amount of energy that remains in each residue is associated with the Amide-I or Amide-II modes. The key to the coherence of the energy transfer is probably the fact that, as the energy pulse passes through a residue, the NH stretch is left very cold, inhibiting energy transfer back in the other direction.

The total Amide-I mode energy, Fig. 10 *c*, shows seven clear maxima, occurring between the maxima of the NH stretch energy, which reflects the presence of two interacting pulses of energy moving down the hydrogen bonded spine.

DISCUSSION

The energy transfer we have observed in this simulation of a section of α-$(Ala)_n$ is qualitatively similar to that observed in the corresponding NMA simulations (2). While this is not surprising given the origin of the α-$(Ala)_n$ force field, one should remember that the character of phase space is very different due to the extension of motion to three dimensions, the altered hydrogen bond geometry, and the increased number of degrees of freedom. Despite this, the resonant mechanism still provides the dominant relaxation pathway.

The critical element of the potential surface is the character of the Amide-I modes. The NH bend amplitude in the Amide-I mode is less in the α-helix surface than in that for NMA, which can be seen in the lower deuterated frequency shift, a slower rate of energy transfer, and a smaller anharmonic coupling constant to balance the rates of inter- and intrapeptide energy transfer. The near optimal value of c_{NHCO} is -3.5 aJ Å^{-3}. This magnitude is plausible, considering the marked

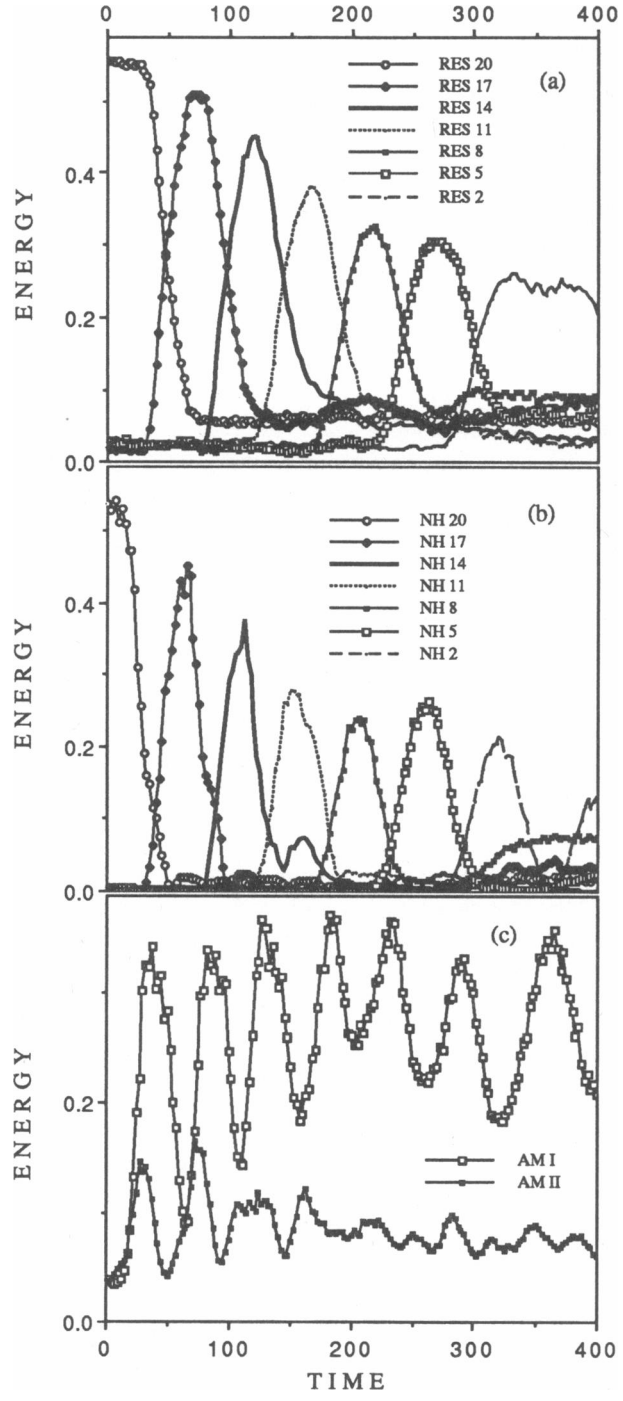

FIGURE 10 As for Fig. 8, using the P_2 surface, for a single trajectory showing efficient energy transfer.

effect of hydrogen bonding on the group frequencies, and considering that a single term represents the effect of several possible couplings. If the NH wagging character of the Amide-I mode were reduced further, the size of the anharmonic constant at the balance point would also be reduced. However, with any decrease in the overall coupling strength, the sensitivity to the balance of the inter-and intrapeptide couplings and also to the frequency mismatch increases. If the amount of NH wagging in the Amide-I mode becomes very small, the range of parameters which allows coherent energy transfer will likewise become very small. However, it should be stressed that there need only be a small amplitude of NH wag in the Amide-I mode for the resonant mechanism to operate.

We have assumed that side chain, intramethyl group and interhelix effects are unimportant. The dominance of the resonance coupling mechanism in very different simulations suggests that it is highly unlikely that these relatively small effects are significant.

At near optimal conditions, the NH stretch frequency of 3,304 cm^{-1} is approximately 25 cm^{-1} away from the experimental band centre for α-$(Ala)_n$ but well within the relatively broad absorption band (many peptides exhibit the NH stretch band centred at $\sim$3,300 cm^{-1}) (38). Moreover, the frequency width of the resonance appears large enough to encompass most of the NH stretch band. This is another measure of the sturdiness of the kinematic part of the resonant energy transfer mechanism. In this regard, we can see the effect of harmonic oscillators, (in place of the anharmonic Morse oscillators used for NMA): the resonance width appears to be at least as large as that seen for NMA even though the kinematic coupling strength has been reduced.

The rate of coherent energy transfer is slightly less than that seen in the NMA simulations. In the best case, the energy pulse reaches a maximum in the last residue by $\sim$3.3 ps, an average velocity of nearly two chain sites per ps. The corresponding quantum rate would therefore be $\sim$3.5 chain sites per ps, or a transfer time between modes of $\sim$0.15 ps. This compares with $\sim$0.1 ps for the NMA simulations (2) and about the same for the simple model (1). This energy transfer rate is manifestly faster than that for any other relaxation pathway.

The dominant mechanism by which energy is lost from the propagating pulse appears, as in NMA (2), to be energy trapping by the Amide-II modes, particularly in the initially excited residue. The NMA simulations showed that this effect is much reduced if the Amide-I mode is initially excited. Thus, it may be that more efficient energy transfer in the helix would be obtained if the Amide-I mode were involved in the initial excitation in conjunction with the NH stretch excitation considered here.

It is clear, from the simulations presented here and previously, that coherent energy propagation is a relatively robust phenomenon, and consequently the ques-

tion of whether this resonance mechanism operates in nature arises.

It is apparent that any experiment probe of crystalline NMA or α-helices will be technically very demanding. Inelastic neutron scattering may possibly be used to observe characteristic effects (2) on the NH stretching phonon frequency dispersion (49), but would be more difficult for protein crystals. The complexity of the vibrational spectrum makes it very hard to envisage an unambiguous manner in which the effects of coherent energy transfer could be observed in the conventional absorption spectrum.

For a test related to the biological context discussed above, site directed mutagenesis could be used to disrupt the hydrogen bonding of an α-helix, say by insertion of a proline residue, between the site of ATP hydrolysis and the ion binding and gate sites. Such an experiment can really only give a negative result (that is disproving the resonant mechanism), if the cellular function is not impaired, the converse would not necessarily prove the hypothesis as interference with the hydrogen bonding may affect the structure and hence the function of many other processes. Similarly, deuteration of an ATPase protein by exposing it to high concentrations of D_2O may have many effects other than destroying the 2:1 resonance. There have been conflicting reports of inhibition of ion transport in D_2O (50, 51). These effects may be due to differences in solvation. FT-IR evidence (52) suggests that the random coil segments of the Ca^{2+} ATPase are deuterated in D_2O, showing an Amide-I frequency shift from 1,657 to 1,643 cm^{-1}. However, the corresponding α-helix and β-sheet frequencies are unchanged, implying no H-D exchange. This is not surprising, because extremely harsh conditions (44) were required to achieve even partial exchange in poly(L-alanine). Generally, the biological effects of D_2O are so large and complex (53) that the role of this resonance mechanism remains an open question.

In this and two previous papers, we have presented a hierarchy of models for the simulation of energy transfer in hydrogen bonded amides and proteins from a simple heuristic model to a comprehensive simulation of a section of α-helix.

The simple model provided a number of useful results. It showed the relationship between the Fermi resonance mechanism and previously studied atomic lattice systems, which leads to coherent energy propagation reminiscent of nonlinear acoustic modes rather than optical modes. Both quantum and classical simulations showed that stable solitonlike pulses of vibrational energy form from the localised excitation and propagate rapidly. Also, the solution of both the classical and quantum equations of motion established the conditions under which the classical simulations provide a good qualitative description of the quantum dynamics, albeit with the rate of energy transfer underestimated by almost a factor of two.

The simulations of energy transfer in NMA and α-$(Ala)_n$ provide a more serious platform for the investigation of the feasibility of the biological hypothesis. By including the exact kinetic energy and comprehensive potential surfaces, these two simulations represent the most complete characterisations attempted of the dynamics of hydrogen bonded amides or peptides. The simulations illustrate that, even though the number of alternative relaxation paths available to the dynamics has increased many-fold, the extended Fermi resonance mechanism dominates. On the basis of these simulations, it can be concluded that coherent energy transfer can occur given two principle requirements: that there is some NH wag amplitude in the Amide-I modes and that the anharmonic potential and kinematic couplings are approximately in balance.

While there is no proof that this resonant mechanism is important in biological systems, it is likely that energy transfer by the Fermi resonances described here forms a feasible relaxation pathway for the types of excitations considered. Furthermore, it is not inconceivable that a biological system, such as an α-helical section of a protein, could have been tuned by evolution to provide a means of highly efficient vibrational energy propagation under conditions similar to those described here.

The authors wish to thank Dr Ronald Pace for valuable discussions on the structure and function of membrane-bound proteins.

We gratefully acknowledge an allocation of computer time on the Fujitsu FACOM VP-100 of the Australian National University Supercomputer Facility.

Received for publication 20 May 1991 and in final form 11 September 1991.

REFERENCES

1. Clarke, D. L., and M. A. Collins. 1990. Simple model of coherent energy transfer by Fermi resonance. *J. Chem. Phys.* 92:5602–5611.
2. Clarke, D. L., and M. A. Collins. 1990. Simulation of coherent energy transfer in a hydrogen bonded amide chain by Fermi resonance. *J. Chem. Phys.* 93:7894–7913.
3. Davydov, A. S. 1982. Biology and Quantum Mechanics. Pergamon Press, Oxford. 185–203.
4. Lomdahl, P. S., and W. C. Kerr. 1985. Do Davydov solitions exist at 300 K? *Phys. Rev. Lett.* 55:1235–1238.
5. Brandl, C. J., N. M. Green, B. Korczak, and D. H. MacLennan. 1986. Two Ca^{2+} ATPase genes: homologies and mechanistic implications of deduced amino acid sequences. *Cell.* 44:597–607.

6. Portillo, F., and R. Serrano. 1988. Dissection of functional domains of the yeast proton-pumping ATPase by directed mutagenesis. *EMBO (Eur. Mol. Biol. Organ.)* 7:1793–1798.
7. Blumenfeld, L. A. 1978. The physical aspects of energy transduction in biological systems. *Q. Rev. Biophys.* 3:251–308.
8. Slater, E. C. 1971. The coupling between energy-yeilding and energy-utilizing reactions in mitochondria. *Q. Rev. Biophys.* 4:35–71.
9. Henderson, R., J. M. Bailwin, T. A. Ceska, F. Zemlin, E. Beckmann, and K. H. Downing. 1990. Model for the structure of bacteriorhodopsin based on high-resolution electron cryomicroscopy. *J. Mol. Biol.* 213:899–929.
10. Deisenhofer, J., O. Epp, K. Miki, R. Huber, and H. Michel. 1985. Structure of the protein subunits in the photosynthetic reaction centre of *Rhodopseudomonas viridis* at 3 Å resolution. *Nature (Lond.).* 318:618–624.
11. Cramer, W. A., W. R. Widger, R. G. Herrmann, and A. Trebst. 1985. Topography and function of thylakoid membrane proteins. *TIBS (Trends Biochem. Sci.).* 10:125–129.
12. Cohen, C., and D. A. D. Parry. 1986. α-Helical coiled coils: a widespread motif in proteins. *TIBS (Trends Biochem. Sci.).* 11:245–248.
13. Green, N. M. 1989. Ions, gates, and channels. *Nature (Lond.).* 339:424–245.
14. Clarke, D. M., T. W. Loo, G. Inesi, and D. H. MacLennan. 1989. Location of high affinity Ca^{2+}-binding sites within the predicted transmembrane domain of the sarco-plasmic reticulum Ca^{2+}ATPase. *Nature (Lond.).* 339:476–478.
15. Serrano, R. 1989. Structure and function of Plasma membrane ATPase. *Annu. Rev. Plant Physiol. Plant Mol. Biol.* 40:61–94.
16. Taylor, W. R., and N. M. Green. 1989. The predicted secondary structures of the nucleotide-binding sites of six cation-transporting ATPases lead to a probable tertiary fold. *Eur. J. Biochem.* 179:241–248.
17. Hol, W. G. J., P. T. van Duijnen, and H. J. C. Berendsen. 1978. The α-helix dipole and the properties of proteins. *Nature (Lond.).* 273:443–446.
18. Wierenga, R. K., M. C. H. De Maeyer, and W. G. J. Hol. 1985. Interaction of pyrophosphate moieties with a-helixes in dinucleotide binding proteins. *Biochemistry.* 24:1346–1357.
19. Clarke, D. M., T. W. Loo, and D. H. MacLennan. 1990. Functional consequences of alterations to amino acids located in the nucleotide binding domain of the Ca^{2+}-ATPase of sarcoplasmic reticulum. *J. Biol. Chem.* 265:22223–22227.
20. Maruyama, K., and D. H. MacLennan. 1988. Mutation of aspartic acid-351, lysine-352, and lysine-515 alters the Ca^{2+} transport activity of the Ca^{2+}-ATPase expressed in COS-1 cells. *Proc. Natl. Acad. Sci. USA.* 85:3314–3318.
21. Maruyama, K., D. M. Clarke, J. Fujii, G. Inesi, T. W. Loo, and D. H. MacLennan. 1989. Functional consequences of alterations to amino acids located in the catalytic center (Isoleucine 348 to Threonine 357) and Nucleotide-binding domain of the Ca^{2+}-ATPase of sarcoplasmic reticulum. *J. Biol. Chem.* 264:13038–13042.
22. Asturias, F. J., and J. K. Blasie. 1991. Location of high-affinity metal binding sites in the profile structure of the Ca^{2+}-ATPase in the sarcoplasmic reticulum by resonance x-ray diffraction. *Biophys. J.* 59:488–502.
23. Bellamy, L. J. 1975. Infrared Spectra of Complex Molecules. Chapman and Hall, London. 231–258.
24. Dollish, F. R., W. G. Fately, and F. F. Bentley, 1974. Characteristic Raman Frequencies of Organic Compounds. John Wiley and Sons, Inc., New York. 121–133.
25. Miyazawa, T. 1960. The characteristic band of secondary amides at 3,100 cm^{-1}. J. Mol. Spectroscopy. 4:168–172.
26. Pivcov, H., B. Schneider, J. Stokr, and J. Jakes. 1964. On the structure and properties of polyamides. XVIII. Temperature changes of the vibrational spectra of *N*-methylacetamide. *Collect. Czech. Chem. Commun.* 29:2436–2448.
27. Schneider, B., A. Horen, H. Pivcov, and J. Honzl. 1965. On the structure and properties of polyamides. XIX. Vibrational spectra of *N*-methylacetamide. *Collect. Czech. Chem. Commun.* 30:2196–2214.
28. Pivcov, H., B. Schneider, and J. Stokr. 1965. On the structure and properties of polyamides. XX. Fermi resonance effects in vibrational spectra of *N*-methylacetamide. *Collect. Czech. Chem. Commun.* 30:2215–2230.
29. Dellepiane, G., S. Abbate, P. Bosi, and G. Zerbi. 1980. Fermi resonances in solid *N*-Methylacetamide. *J. Chem. Phys.* 73:1040–1047.
30. Katz, J. L., and B. Post. 1960. The crystal structure of *N*-methyl acetamide. *Acta Crystallogr.* 13:624–628.
31. Sibert, E. L., III, W. P. Reinhardt, and J. T. Hynes. 1982. Intramolecular vibrational relaxation of CH overtones of benzene. *Chem. Phys. Lett.* 92:455–458.
32. Sibert, E. L., III, W. P. Reinhardt, and J. T. Hynes. 1984. Intramolecular vibrational relaxation of CH overtones of benzene. *J. Chem. Phys.* 81:1115–1134.
33. Sibert, E. L., III, J. T. Hynes, and W. P. Reinhardt. 1984. Classical dynamics of highly excited CH and CD overtones in benzene and perdeuterobenzene. *J. Chem. Phys.* 81:1135–1144.
34. Némethy, G., D. C. Phillips, S. J. Leach, and H. A. Scheraga. 1967. A second right handed helical structure with parameters of the Pauling-Corey α helix. *Nature (Lond.).* 214:363–365.
35. Dwivedi, A. M., and S. Krimm. 1984. Vibrational analysis of peptides, polypeptides and proteins. XVIII. Conformational sensitivity of the α helix spectrum: ai- and aii-poly-L-alanine. *Biopolymers.* 23:923–943.
36. Arnott, S., and S. D. Dover. 1967. Refinement of bond angles of an α helix. *J. Mol. Biol.* 30:209–212.
37. Dwivedi, A. M., and S. Krimm. 1984. Vibrational analysis of peptides, polypeptides and proteins. 19. Force fields for α helix and β sheet structures in a side-chain point-mass approximation. *J. Phys. Chem.* 88:620–627.
38. Krimm, S., and J. Bandekar. 1986. Vibrational spectroscopy and conformations of peptides, polypeptides and proteins. *Adv. Protein Chem.* 38:181–364.
39. Krimm, S., and Y. Abe. 1972. Intermolecular interaction effects in Amide-I vibrations of β polypeptides. *Proc. Natl. Acad. Sci. USA.* 69:2788–2792.
40. Jorgensen, W. L., and C. J. Swenson. 1985. Optimized intermolecular potential functions for amides and peptides. Structure and properties of liquid amides. *J. Am. Chem. Soc.* 107:569–578.
41. Sugawara, Y., A. Y. Hirakawa, and M. Tsuboi. 1984. In-plane force constants of the peptide group: least squares adjustment starting from ab initio values of *N*-Methylacetamide. *J. Mol. Spectroscopy.* 108:206–214.
42. Sugawara, Y., A. Y. Hirakawa, M. Tsuboi, S. Kato, and K. Morokuma. 1986. Ab initio SCF MO study of the force fields of amides. *J. Mol. Spectroscopy.* 115:21–33.
43. Balázs, A. 1987. A comparative ab initio study of amides. Part II. Force fields and vibrational assignments for *N*-methylacetamide

and cis-*N*-methylacetamide. *J. Mol. Structure (Theochem).* 153: 103–120.

44. Rabolt, J. F., W. H. Moore, and S. Krimm. 1977. Vibrational analysis of peptides, polypeptides and proteins. 3. α-poly(L-alanine). *Macromolecules.* 10:1065–1074.
45. Frushour, B. G., and J. L. Koenig. 1974. Raman spectroscopic study of mechanically deformed poly-L-alanine. *Biopolymers.* 13:455–474.
46. Tipping, M., K. Viras, and T. A. King. 1984. Low-frequency dynamics of solid poly(L-alanine) from Raman spectroscopy. *Biopolymers.* 23:2891–2899.
47. Pulay, P., G. Fogarasi, and J. E. Boggs. 1981. Force field, dipole moment derivatives and vibronic constants of benzene from a combination of experimental and ab initio quantum chemical information. *J. Chem. Phys.* 74:3999–4014.
48. Mortenson, O. S., B. R. Henry, and M. A. Mohammadi. 1981. The effect of symmetry within the local mode picture: a reanalysis of the overtone spectra of the dihalomethanes. *J. Chem. Phys.* 75:4800–4808.
49. Hirst, P. H., L. M. Needham, A. D. Taylor, Z. A. Bowden, and J. W. White. 1989. High-energy neutron inelastic scattering from adsorbed hydrogen molecules. *Chem. Phys.* 135:457–466.
50. Lobyshev, V. I., J. Vogel', L. V. Yakovenko, M. I. Rezayeva, and V. A. Tverdislov. 1982. D_2O as a modifier of ionic specificity of Na, K-ATPase. *Biophysics.* 27:614–624.
51. Huxtable, R., and R. Bressler. 1974. The effect of deuterium ion concentration on the properties of sarcoplasmic reticulum. *J. Membr. Biol.* 17:189–197.
52. Rodriguez-Arrondo, J. L., and F. M. Goni. 1985. A study of sarcoplasmic reticulum protein conformations in H_2O and D_2O by Fourier-transform infrared spectroscopy. *Spectroscopy of Biological Molecules Proc. 1st Eur. Conf.* A. J. P. Alix, L. Bernard and M. Manfait, editors. John Wiley and Sons, Inc., 184–186.
53. Katz, J. J., and H. L. Crespi. 1970. Isotope effects in biological systems. *In* Isotope Effects in Chemical Reactions. C. J. Collins and N. S. Bowman, editors. Van Nostrand Reinhold Company, New York. 286–363.